Available online at www.sciencedirect.com
SCIENCE DIRECT®
Journal of Computational Physics 206 (2005) 6–15
JOURNAL OF COMPUTATIONAL PHYSICS
www.elsevier.com/locate/jcp

Short Note

Interaction of a shock with a density disturbance via shock fitting

Ambady Suresh

QSS Group Inc., NASA Glenn Research Center, 21000 Brookpark Road, MS 142-4, Cleveland, OH 44135, USA

Received 26 August 2004; received in revised form 23 November 2004; accepted 23 November 2004
Available online 24 January 2005

Abstract

An accurate solution to the problem of a normal shock moving into still fluid with a density variation is presented. The solution is obtained using a shock fitted approach and Runge–Kutta time integration. Uniform third order accuracy of the scheme is demonstrated. Comparisons with shock captured solutions show that the fitted solution presented here is more accurate.

Keywords: Shock capturing; Shock fitting; Exact solutions

1. Introduction

The problem of a normal shock moving into still air with a density variation has proved to be a nice test problem for shock-capturing schemes because it has both smooth structure and moving discontinuities. This problem was first proposed by Shu and Osher [1] in 1989 and has become a standard test case for shock capturing schemes. In contrast to other test problems, such as the shock tube problems of Sod and Lax, this problem is a good test of the spatial accuracy of a numerical scheme in smooth regions.

Its one drawback, which we wish to address here, is that there is no exact solution. A linearized solution of this problem, in terms of plane waves, may be found in [2] but is not of much use in validating numerical solutions because, for the parameters used, the problem is nonlinear. In current practice, a solution on a very fine mesh by a shock capturing scheme is used as an exact solution, but, as we show in this paper, even on very fine grids these schemes display spurious oscillations.

E-mail address: ambady.suresh@grc.nasa.gov.

0021-9991/$ - see front matter
doi:10.1016/j.jcp.2004.11.036

As the shock propagates into the varying density field, an oscillatory solution develops behind the shock. At any instant of time, this oscillatory solution is bounded by an expansion fan on the left, a contact discontinuity in the middle and the traveling shock on the right (see Fig. 2) . In time, this oscillatory solution steepens to form a shock train behind the shock, but for earlier times, the solution behind the shock remains continuous.

Our aim in this paper is to present a highly accurate solution to this problem during this early time period using a shock fitted approach. In this approach, the shock front is a computational boundary whose trajectory is generated during the calculation. Since the flow in the computational domain is smooth, there is good reason to expect a shock fitted solution to be highly accurate. In fact, we modify the problem slightly so that the early time solution is a bit smoother than the original problem (see below).

Shock fitted solutions have been widely [3–8] used to obtain highly accurate solutions.The main advantage of shock fitting is that simpler, more accurate numerical schemes can be used without incurring spurious O(1) errors at the shock. However, they can be used only in special circumstances where the shock structure is simple and known in advance. Some previous applications have included the interaction of sound and vorticity waves with a stationary shock, a blunt body in supersonic flow, shock reflection problems in two dimensions etc.

We present the shock fitted solution next. Grid refinement studies to estimate the absolute truncation error and comparisons with shock capturing schemes are presented thereafter, where it is shown that the shock fitted solution is more accurate.

2. Shock fitted solution

The original problem can be stated on the domain $[-1,1]$ as follows: At $t = 0$, a normal shock of shock Mach number M at $x = x_0$, is moving to the right into still air with a density profile. For $x \leqslant x_0$, we have

$$\begin{aligned} \rho &= ((\gamma+1)M^2)/((\gamma-1)M^2+2), \\ u &= 2(\gamma)^{1/2}(M^2-1)/((\gamma+1)M), \\ p &= 1.0 + 2\gamma(M^2-1)/(\gamma+1), \end{aligned} \tag{1}$$

while for $x > x_0$, we have

$$\begin{aligned} \rho &= 1.0 + \epsilon \sin[5\pi x], \\ u &= 0, \\ p &= 1. \end{aligned} \tag{2}$$

This problem is usually solved with the following values for the parameters: $\gamma = 1.4$, $M = 3$, $\epsilon = 0.2$, $x_0 = -0.8$ and the final solution is obtained at $t = 0.36$.

Since the shock fitted solution works best in smooth regions, we modify the problem slightly so that the solution behind the traveling shock is smoother. Instead of (2) we set (for $x > x_0$)

$$\begin{aligned} \rho &= 1.0 + \epsilon \sin[2.5\pi x]^4, \\ u &= 0, \\ p &= 1. \end{aligned} \tag{3}$$

In the original problem, ρ_x for $x > x_0$ is nonzero while in the modified problem ρ_x, ρ_{xx} and ρ_{xxx} are zero. This modification imposes a gentle start to the interaction and has the effect of smoothing over the expansion fan and the contact discontinuity in the region behind the shock. At the same time, it retains all the basic features of the solution, namely a highly oscillatory field followed by a traveling shock.

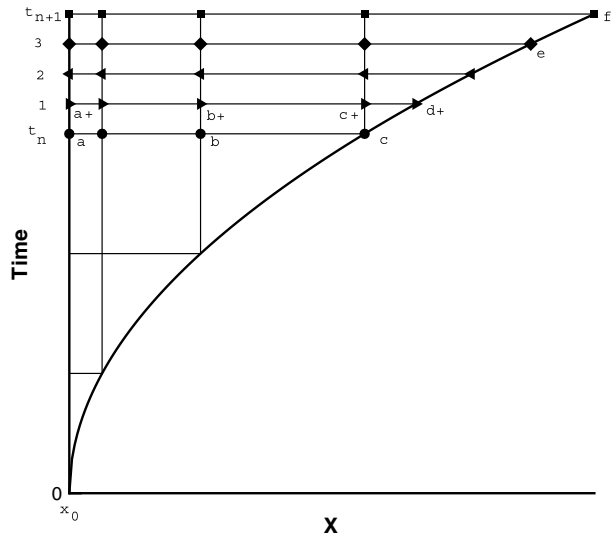

Fig. 1. Computational grid and update procedure for the shock fitted solution.

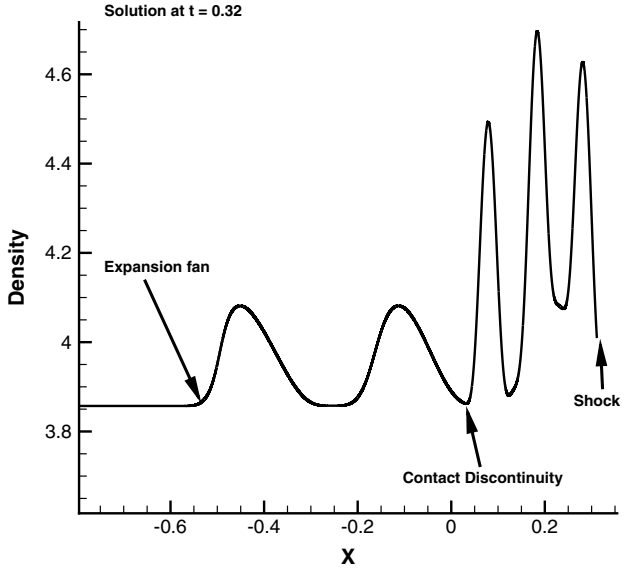

Fig. 2. Solution on a fine grid for $t = 0.32$; $\Delta t = 6.25\text{E} - 6$.

The shock fitted solution is obtained on a nonuniform grid that is traced out by the motion of the shock. At a time level $t_n = n\Delta t$, the nodes are given by x_i, $i = 1, n + 1$. x_{n+1} is the shock location at t_n and x_i, $1 \leqslant i \leqslant n$ are the previous shock locations at time levels, $(i - 1)\Delta t$. This grid is shown in Fig. 1.

The key observation to be made in obtaining the shock fitted solution is that conditions behind the shock remain supersonic throughout the interaction. This permits a solution on the above grid that is updated

from left to right using a fixed upwind biased stencil. In other words, the interior nodes are updated first, starting from the left boundary, and the shock position updated last.

Since the grid is not uniform, and the variables are smooth we solve the one dimensional Euler equations in primitive (nonconservative) form

$$\begin{aligned} &\rho_t + u\rho_x + \rho u_x = 0, \\ &u_t + uu_x + p_x/\rho = 0, \\ &p_t + \gamma p u_x + up_x = 0, \end{aligned} \tag{4}$$

where (ρ,u,p), are the density, velocity and pressure respectively; $\gamma = 1.4$, is the ratio of specific heats.

As the shock wave propagates one cell every time step, the CFL limit λ is necessarily greater than one since,

$$\lambda = (|u| + a)\Delta t/\Delta x = (|u| + a)/U_s > 1, \tag{5}$$

where U_s is the shock speed. Thus we have to choose a scheme that remains stable for CFL numbers greater than unity [3]. The usual choice is an implicit scheme, but in the interest of simplicity we explore an explicit scheme with Runge–Kutta time stepping.

Let $v^n = (\rho^n,u^n,p^n)$ denote the primitive variables at time level n and $f(t,v^n)$ denote the time derivatives at time level n. We choose the standard four stage Runge–Kutta scheme for this purpose, given by

$$\begin{aligned} k_1 &= \Delta t f(t_n, v^n), \\ k_2 &= \Delta t f(t_n + \Delta t/2, v^n + k_1/2), \\ k_3 &= \Delta t f(t_n + \Delta t/2, v^n + k_2/2), \\ k_4 &= \Delta t f(t_n + \Delta t, v^n + k_3), \\ v^{n+1} &= v^n + (k_1 + 2k_2 + 2k_3 + k_4)/6. \end{aligned} \tag{6}$$

Next, we discuss the spatial discretization of Eq. (4). Since the flow conditions remain supersonic, a one point upwind biased stencil is a natural choice for stability. With the above time discretization, to be stable at CFL numbers greater than unity, the maximum order possible is three. Thus,we use the one point upwind stencil $(x_{i-2}, x_{i-1}, x_i, x_{i+1})$ for the derivative at node x_i, $1 \leqslant i \leqslant n$. For $i = n + 1$, we use the fully upwind stencil $(x_{i-3}, x_{i-2}, x_{i-1}, x_i)$. On a uniform grid, the above scheme with the one point upwind stencil is stable and uniformly third order accurate for CFL numbers $\lambda < 1.753$, which is adequate for our purpose. The left boundary is supersonic during the whole interaction and therefore all variables are held fixed there. For ease of coding, ghost cells are added at the left boundary so that the boundary cells can be updated just as interior cells.

To preserve third order accuracy of the whole scheme, the shock trajectory is also integrated using the same Runge–Kutta scheme. At every stage, the interior nodes are advanced first into the next stage. Next, the shock node (i.e. x_{n+1}, at time level n) is advanced into the next stage using the existing shock velocity at time level n. With the shock location known, the primitive variables at the new shock location are obtained by extrapolation (third order) from the interior nodes. With conditions known on both sides of the discontinuity, a Riemann problem [9] is solved to obtain the shock velocity at that stage. This procedure yields a shock velocity at every stage which is then used to obtain the shock position at the next time level. At the final stage, the shock node is set to the post-shock conditions which are available from the Riemann problem solution, which is obtained as described in [9].

This update procedure can be summarized with respect to Fig. 1, as follows: It is assumed that all variables, including the shock speed are known at time level t^n.

1. The nodes a to b at time level t^n are advanced into the first Runge–Kutta stage as per (6) using the one point upwind biased stencil.
2. Node c is advanced to the next stage by the fully upwind stencil.
3. The shock location at the next stage ($d+$) is obtained from the known shock velocity at c. Values of the primitive variables are extrapolated from the interior values at this stage ($a+$, $b+$, $c+$) to the new shock location $d+$. A Riemann problem is solved here with the left state being the extrapolated value and the right state being the given initial condition. The new shock velocity at $d+$ is obtained from the Riemann solution.
4. The same procedure is used to update the solution from stage 1 to stage 2 and stage 2 to stage 3.
5. In the final update, from stage 3 to time level t^{n+1}, the interior nodes and shock location are updated as per the Runge–Kutta formula (6). The new shock velocity at the new shock location (f) is obtained by solving the Riemann problem as before. Finally, the primitive variables at the new shock location (f) are set to the post-shock variables of the Riemann problem solution.

This concludes the description of the shock fitted scheme. In the next section we present some grid convergence studies on this scheme as well as comparisons with traditional shock capturing schemes.

3. Numerical results and comparisons

We examine the solution obtained at $t = 0.32$, when the solution is still continuous behind the shock. A typical solution on a very fine grid is shown in Fig. 2.

3.1. Grid refinement studies

We first calculate the relative truncation error in these solutions by subtracting a fine grid ($\Delta t/2$) solution from the coarse grid solution (Δt) on the shock trajectory. For example, if we denote the coarse grid solution at node i as $u_h(i)$, the fine grid solution at the same location as $u_{h/2}(2i-1)$, the difference in the Max norm is

$$e(h) = \mathrm{Max}_i |u_h(i) - u_{h/2}(2i-1)|. \tag{7}$$

Table 1
Grid refinement on shock trajectory

$h = \Delta t$	$L_\infty(u_h - u_{h/2})$	m_∞	$L_1(u_h - u_{h/2})$	m_{L1}
0.32E − 2	0.4614E − 2	0.2025E + 1	0.7157E − 3	0.1816E + 1
0.16E − 2	0.1134E − 2	0.2652E + 1	0.2032E − 3	0.2876E + 1
0.8E − 3	0.1805E − 3	0.2966E + 1	0.2768E − 4	0.2995E + 1
0.4E − 3	0.2310E − 4	0.2998E + 1	0.3471E − 5	0.2990E + 1
0.2E − 3	0.2891E − 5	0.3000E + 1	0.4369E − 6	0.2993E + 1
0.1E − 3	0.3614E − 6	0.3000E + 1	0.5487E − 7	0.2996E + 1
0.5E − 4	0.4517E − 7	0.3000E + 1	0.6877E − 8	0.2998E + 1
0.25E − 4	0.5646E − 8	0.3002E + 1	0.8609E − 9	0.3001E + 1
0.125E − 4	0.7050E − 9	–	0.1075E − 9	–

Table 2
Grid refinement at $t = 0.32$

$h = \Delta t$	$L_\infty(u_h - u_{h/2})$	m_∞	$L_1(u_h - u_{h/2})$	m_{L1}
0.32E − 2	0.1387E − 0	0.7832E + 0	0.6424E − 2	0.1409E + 1
0.16E − 2	0.8062E − 1	0.2171E + 1	0.2420E − 2	0.2155E + 1
0.8E − 3	0.1790E − 1	0.2755E + 1	0.5431E − 3	0.2789E + 1
0.4E − 3	0.2652E − 2	0.2938E + 1	0.7857E − 4	0.2946E + 1
0.2E − 3	0.3459E − 3	0.2984E + 1	0.1019E − 4	0.2983E + 1
0.1E − 3	0.4373E − 4	0.2995E + 1	0.1289E − 5	0.2993E + 1
0.5E − 4	0.5485E − 5	0.2998E + 1	0.1619E − 6	0.2997E + 1
0.25E − 4	0.6867E − 6	0.2999E + 1	0.2029E − 7	0.2997E + 1
0.125E − 4	0.8590E − 7	–	0.2541E − 8	–

This difference is approximately the true truncation error (albeit, multiplied by a factor of $1 - 2^{(-m)}$, where m is the order of the scheme). Using two such differences (i.e. three levels of grids) we can also compute the order of accuracy, m, as

$$m = \ln[e(h)/e(h/2)]/\ln(2). \tag{8}$$

In Table 1, we present these differences and the order of accuracy in the L_1 and Max norms on various coarse grids. Note that the errors are computed over five fields, namely, the shock position, density, velocity, pressure and shock velocity. It can be seen that the computed order of accuracy approaches the formal design accuracy of the scheme in both norms and the relative truncation error estimate falls to within $O(10^{-9})$.

In Table 2, we examine the interior solution, i.e. at the final time level in space. Since the spatial grids are nonuniform, the fine grid solution is interpolated on to the coarse grid node using a centered cubic interpolation. The differences between these solutions and order of accuracy are computed as above and shown in Table 2.

Again, the order of accuracy of the interior solution does approach the formal order of accuracy of the scheme in both norms showing that the scheme is uniformly third order accurate. The relative errors obtained here are slightly higher than those obtained on the shock trajectory.

We remark that the order of accuracy obtained for shock fitted solutions using the original initial condition (i.e. with (2) rather than (3)) is between third. and second order in the L_1 norm for the spatial solution. However, in the Max norm, the order of accuracy degrades to between zeroth. and first order due to errors at the expansion fan and contact discontinuity. This is to be expected as the solution is not smooth at these locations.

3.2. Comparison with shock capturing schemes

The interior solution can be compared with results from shock capturing schemes.We have chosen to compare results with the WENO scheme of Jiang and Shu [10] and the MP5 scheme of Suresh and Huynh [11]. Both these schemes are formally third order in time and fifth order in space and have been validated on a number of problems. Since these schemes are well known, we do not describe them here but refer the reader to the above references.

Table 3 shows grid refinement studies on the shock captured solution obtained with WENO5 and MP5 schemes. For shock capturing schemes, it does not make sense to compute errors on the Max norm due to the O(1) errors at the shock. Therefore, only the L_1 errors are shown.

The relative truncation errors obtained are several orders of magnitude greater than those obtained with the shock fit solution. The order of accuracy is a noisy function of grid resolution and nowhere near the

Table 3
MP5 and WENO5 solutions at $t = 0.32$. CFL = 0.4

Δx	MP5		WENO5	
	$L_1(u_h - u_{h/2})$	m_{L1}	$L_1(u_h - u_{h/2})$	m_{L1}
0.200E − 1	0.2828E − 1	0.1955E + 1	0.3235E − 1	0.1528E + 1
0.100E − 1	0.7295E − 2	0.7979E + 1	0.1122E − 1	0.9448E + 0
0.500E − 2	0.4196E − 2	0.4642E + 0	0.5829E − 2	0.8222E + 0
0.250E − 2	0.3041E − 3	0.1875E + 0	0.3297E − 2	0.1713E + 1
0.125E − 2	0.8294E − 3	0.8894E + 0	0.1006E − 2	0.9661E + 0
0.625E − 3	0.4477E − 3	0.7882E + 0	0.5147E − 3	0.9016E + 0
0.3125E − 3	0.2593E − 3	0.5333E + 0	0.2755E − 3	0.7413E + 0
0.15625E − 3	0.1791E − 3	–	0.1648E − 3	–

formal third order accuracy of both schemes. To reduce the possibility of coding error, both these schemes were tested on smooth initial conditions (i.e. p, $u = 1.0$ and $\rho = \rho(x)$, where $\rho(x)$ is smooth) and returned between third and fifth order accuracy as expected.

The actual order of accuracy achieved by a shock capturing scheme in the presence of moving shocks has been the subject of many studies [12–16]. For example, Casper et al. [15] study a sound shock interaction problem using a higher order shock capturing scheme and find only first order convergence downstream of the shock. Higher order convergence is restored if some form of sub-cell resolution is used. In general, the consensus is that regardless of the formal order of accuracy of the scheme, only first order accuracy is achieved in regions downstream of the unsteady shock.

In light of these results, the results of Table 3 are not surprising. Here, the lower order convergence is observed in a region that is again downstream of the traveling shock in the shock fixed frame.

Of some interest is also the maximum value attained in these post shock oscillations. Schemes with lower accuracy in smooth regions will tend to damp out these oscillations resulting in lower maximum values. Table 4 shows the maximum values attained on various grids for the shock fitted scheme and the two shock capturing schemes described above. The maximum value is obtained via a cubic fit of the nodal data.

Finally, we compare these solutions in the vicinity of the contact and expansion fan. Fig. 3 shows fine grid solutions in the vicinity of the contact discontinuity. The second and higher order shock captured solutions show tiny spurious oscillations on the order of 0.02 here. Although we do not have the exact solution, it is quite clear that the shock fitted solution is more accurate here.This is also true for Fig. 4 which shows the solution in the vicinity of the expansion fan.

Table 4
Maximum values of density at $t = 0.32$

N	SFIT	MP5	WENO5
100	4.5736731336	4.5006636946	4.3342233874
200	4.6300521471	4.6043947700	4.5319666062
400	4.6844077681	4.6827825688	4.6586656371
800	4.6945802422	4.6957858570	4.6871419691
1600	4.6959239148	4.6999711656	4.6932034039
3200	4.6960953911	4.7020154337	4.6950582082
6400	4.6961170390	4.6990172028	4.6956734114
12,800	4.6961197579	4.6970758461	4.6958732793
25,600	4.6961200986	4.6962524165	4.6959337856
51,200	4.6961201412	–	–

For the shock fitted solution (SFIT), $\Delta t = 0.32/N$, for all others, $\Delta x = 2/N$.

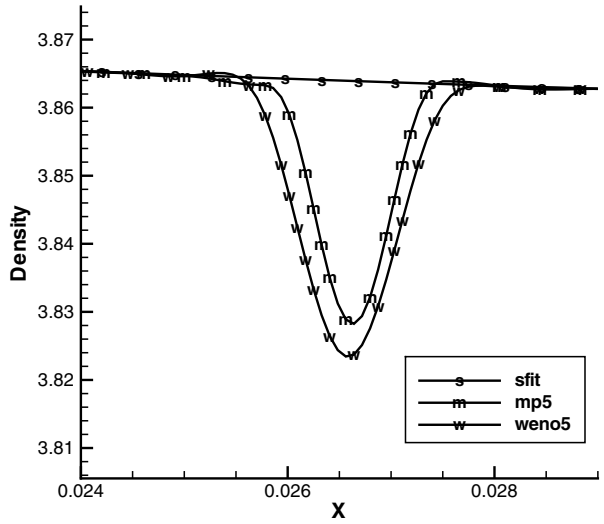

Fig. 3. Solution near the contact discontinuity ($t = 0.32$). For SFIT $\Delta t = 6.25\text{E} - 6$, for WENO5 and MP5, $\Delta x = 7.8125\text{E} - 5$, CFL = 0.4.

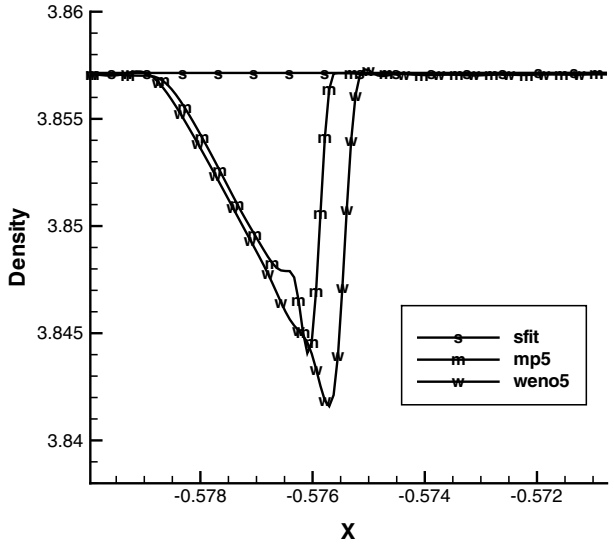

Fig. 4. Solution near the expansion fan ($t = 0.32$). For SFIT $\Delta t = 6.25\text{E} - 6$, for WENO5 and MP5, $\Delta x = 7.8125\text{E} - 5$, CFL = 0.4.

3.3. Tables of the solution

For comparison purposes, Table 5(a) provides the solution on the shock trajectory (i.e. in time) at a few discrete points. Similarly, Table 5(b) presents the spatial solution at $t = 0.32$ at a few points. These points include all the local extrema in the density solution and the locations of the fan, contact and shock (see Fig. 2).

Table 5
(a) Solution on the shock trajectory[a]

t	x_s	ρ_s	u_s	p_s
0.000E + 00	−0.8000000000E + 00	0.3857142857E + 01	0.2629368792E + 01	0.1033333333E + 02
0.320E − 01	−0.6869511634E + 00	0.4180936854E + 01	0.2587267764E + 01	0.1065541386E + 02
0.640E − 01	−0.5780236495E + 00	0.4704043025E + 01	0.2525691427E + 01	0.1114326261E + 02
0.960E − 01	−0.4673536863E + 00	0.3912532449E + 01	0.2618746150E + 01	0.1037369215E + 02
0.128E + 00	−0.3539376770E + 00	0.3868308546E + 01	0.2624136941E + 01	0.1032619633E + 02
0.160E + 00	−0.2423929221E + 00	0.4571701754E + 01	0.2538586295E + 01	0.1101208886E + 02
0.192E + 00	−0.1339597919E + 00	0.4364662937E + 01	0.2562232416E + 01	0.1081713872E + 02
0.224E + 00	−0.2154566429E − 01	0.3855261929E + 01	0.2626175691E + 01	0.1031429159E + 02
0.256E + 00	0.9173603049E − 01	0.4024728380E + 01	0.2605222244E + 01	0.1049221472E + 02
0.288E + 00	0.2014046538E + 00	0.4758217839E + 01	0.2521482952E + 01	0.1120191140E + 02
0.320E + 00	0.3112355137E + 00	0.4009171859E + 01	0.2609686589E + 01	0.1048922702E + 02

(b) Solution at $t = 0.32$

x	ρ	u	p
−0.8000000000E + 00	0.3857142857E + 01	0.2629368792E + 01	0.1033333333E + 02
−0.5780447709E + 00	0.3857142857E + 01	0.2629368792E + 01	0.1033333333E + 02
−0.4512996452E + 00	0.4081523815E + 01	0.2519241880E + 01	0.1118458036E + 02
−0.2487365100E + 00	0.3857724205E + 01	0.2629076918E + 01	0.1033551381E + 02
−0.1126873543E + 00	0.4081576804E + 01	0.2519216451E + 01	0.1118478365E + 02
0.3220387877E − 01	0.3861974296E + 01	0.2627200628E + 01	0.1034954005E + 02
0.7909342628E − 01	0.4493197701E + 01	0.2629082704E + 01	0.1033366584E + 02
0.1230115892E + 00	0.3880910514E + 01	0.2618276560E + 01	0.1040211607E + 02
0.1838852235E + 00	0.4696120028E + 01	0.2541721870E + 01	0.1099365631E + 02
0.2401756463E + 00	0.4074588328E + 01	0.2527051395E + 01	0.1113809055E + 02
0.2808749867E + 00	0.4627263910E + 01	0.2572520017E + 01	0.1078050825E + 02
0.3112355137E + 00	0.4009171859E + 01	0.2609686589E + 01	0.1048922702E + 02

[a] x_s is the shock location, while ρ_s, u_s, p_s are the density, velocity, and pressure on the left side of the shock.

4. Conclusions

A simple and inexpensive scheme to compute the solution of a normal shock interacting with a varying density field was presented. The shock fitted solution appears to be more accurate than several state of the art shock capturing solutions. It is hoped that this shock fitted solution can be used in place of an exact solution on this problem.

Preliminary comparisons between the shock fitted solutions and the shock captured solutions raise several interesting questions. On this problem, the shock capturing schemes incur small spurious oscillations near the expansion fan and contact discontinuity, even on very fine grids. In addition, it appears that the shock capturing schemes achieve lower order accuracy behind the traveling shock, similar to previous studies. It remains to be seen whether higher order accuracy can be achieved with some form of sub-cell resolution.

In the context of evaluating numerical solutions, the goal is to obtain a highly accurate numerical solution, where for example, the change in the solution from coarse grid to fine grid is on the order of machine accuracy (10^{-12} for double precision). While we are still far from that goal, the shock fitted solutions presented here are a step toward that goal.

Acknowledgments

The author thanks H.T. Huynh for several interesting discussions during the course of this paper. The author is also grateful to the Computing and Interdisciplinary Systems Office at NASA Glenn Research Center for permission to publish this work.

References

[1] C.-W. Shu, S. Osher, Efficient implementation of essentially nonoscillatory schemes, II, J. Comput. Phys. 83 (1989) 32.
[2] J. McKenzie, K. Westphal, Phys. Fluids 11 (1968) 2350.
[3] B.L. Rozdestvenskii, N.N. Janenko, Systems of quasilinear equations and their applications to gas dynamicsTranslations of Mathematical Monographs, vol. 55, American Mathematical Society, Providence Rhode Island, 1980.
[4] D.A. Kopriva, T.A. Zang, M.Y. Hussaini, Spectral methods for the Euler equations: the blunt body problem revisited, AIAA J. 29 (1991) 1458.
[5] D.A. Kopriva, Shock fitted multidomain solution of supersonic flows, Comput. Meth. Appl. Mech. Eng. 175 (1999).
[6] M.D. Salas, T.A. Zang, M.Y. Hussaini, Shock-fitted Euler solutions to shock–vortex interactions, in: E. Krause (Ed.), Proc. 8th. Int. Conf. Numerical Methods in Fluid Dynamics, Springer, Berlin, 1982, p. 461.
[7] M.Y. Hussaini, D.A. Kopriva, M.D. Salas, T.A. Zang, Spectral methods for the Euler equations: Part 2. Chebyshev methods and shock fitting, AIAA J. 23 (1985) 234.
[8] C. Canuto, M.Y. Hussaini, A. Quarteroni, T.A. Zang, Spectral Methods in Fluid Dynamics, Springer-Verlag, Berlin, 1988, p. 266.
[9] J.J. Gottlieb, C.P.T. Groth, Assessment of Riemann solvers for unsteady one-dimensional inviscid flows of a perfect gas, J. Comput. Phys. 78 (1988) 437.
[10] G.-S. Jiang, C.-W. Shu, Efficient implementation of weighted ENO schemes, J. Comput. Phys. 126 (1996) 202.
[11] A. Suresh, H.T. Huynh, Accurate monotonicity preserving schemes with Runge–Kutta time stepping, J. Comput. Phys. 136 (1997) 83.
[12] A. Majda, S. Osher, Propagation of error in regions of smoothness for accurate difference approximations to hyperbolic equations, Commun. Pure Appl. Math. 30 (1977) 671.
[13] M.S. Mock, P.D. Lax, The computation of discontinuous solutions of linear hyperbolic equations, Commun. Pure Appl. Math. 31 (1978) 423.
[14] B. Engquist, B. Sjogreen, The convergence rate of finite difference schemes in the presence of shocks, SIAM J. Numer. Anal. 35 (1998) 2464.
[15] J. Casper, M.H. Carpenter, Computational considerations for the simulation of shock-induced sound, SIAM J. Sci. Comput. 19 (1998) 813.
[16] M.H. Carpenter, J.H. Casper, Accuracy of shock capturing in two spatial dimensions, AIAA J. 37 (1999) 1072.